Optimization of trajectory tracking accuracy and vibration suppression for continuum flexible robotic arm

Haiyan Sun[1], Yuanyuan Li[2]
College of Information Science and Engineering, Qingdao Huanghai University, Qingdao, China
[1]Corresponding author
E-mail: [1]*hysun2603@sina.com*, [2]*yuanli_2605@sina.com*

Received 4 May 2026; accepted 2 August 2026; published online 27 August 2026
DOI https://doi.org/10.21595/jve.2026.26644

Check for updates

Copyright © 2026 Haiyan Sun, et al. This is an open access article distributed under the Creative Commons Attribution License, which permits unrestricted use, distribution, and reproduction in any medium, provided the original work is properly cited.

Abstract. Drawbacks of continuous flexible manipulators, such as insufficient trajectory tracking accuracy and obvious flexible vibration, were targeted, and an integrated hierarchical strategy of trajectory replanning and disturbance rejection control was proposed for cable-driven flexible manipulators. A STO-MPC (Stochastic Trajectory Optimization Model Predictive Control) framework was constructed. Probabilistic obstacle avoidance constraints and gradient-independent solving mechanisms were introduced to tackle the high computational delay and poor dynamic adaptability of traditional planning approaches, while stiffness constraints and residual vibration suppression requirements of flexible structures were fully satisfied. A cooperative control framework of ADO-RITSMC (Adaptive Disturbance Observer-Rapid Integral Terminal Sliding Mode Control) was established. Model-free real-time compensation for multi-source disturbances was realized, finite-time convergence of tracking errors was achieved by the improved terminal sliding mode, and residual vibration of flexible links was effectively suppressed accordingly. Comprehensive comparative tests were conducted on standard O-shaped trajectories and high-curvature V-shaped trajectories, with GO-MPC (Gaussian Observer-based Model Predictive Control), APF-MPC (Artificial Potential Field-based Model Predictive Control) sliding mode algorithms. Experimental results demonstrated that STO-MPC can achieve the lowest peak computation time, completes the convergence of obstacle state estimation within 0.5 s, and yields a steady-state velocity estimation error of 0.0015 m/s. Its trajectory tracking RMSE (Root Mean Square Error) is 18.7 % and 36.8 % lower than that of GO-MPC and APF-MPC respectively, delivering superior real-time performance, estimation stability and tracking accuracy. The proposed ADO-RITSMC reduces vibration amplitude by 16.7 % with a peak vibration acceleration of –1.0 g, and exhibits faster vibration attenuation and slighter trajectory oscillation during dynamic obstacle avoidance, which fully verifies the hierarchical collaborative advantages of STO-MPC trajectory replanning and ADO-RITSMC vibration suppression.

Keywords: flexible manipulator, model predictive control, trajectory replanning, dynamic obstacle avoidance, vibration suppression.

Nomenclature

MPC	Model predictive control
STO-MPC	Stochastic trajectory optimization model predictive control
ADO-RITSMC	Adaptive disturbance observer-rapid integral terminal sliding mode control
GO-MPC	Gaussian observer-based model predictive control
APF-MPC	Artificial potential field-based model predictive control
FNTSMC	Fast non-singular terminal sliding mode control
ESO	Extended state observer
NDOs	Nonlinear disturbance observers
BS-NLO	Backstepping-based nonlinear disturbance observer

ISSN PRINT 1392-8716, ISSN ONLINE 2538-8460

RMSE	Root mean square error
MAE	Mean absolute error
MaxAE	Maximum absolute error
θ	Spatial bending angle
α	Rotation angle
w	Workspace position vector
h	Joint space configuration vector
ζ	Curvature radius measured from the center
ζ_i	Bending curvature radius of the i-th driving rope
r	The distance between the center of the disc and the center of each routing hole
α_i	The rotation angle of the i-th driving rope
Q	Inertia matrix
F	Matrix of Coriolis force and centrifugal force
E	The vector of gravity term
ψ_f	The flexible effect vector
ψ	The generalized force input vector
h_d	The desired position vector
e	Trajectory error matrix
$V_{oj}(k)$	The nearest distance from the jth obstacle to the end-effector
ζ_{oj}	The velocity variation rate of the jth obstacle
A_o	Weight coefficient
$d_{j,o}$	The distance between the flexible manipulator and the j-th obstacle
$d_{j,o}^*$	Actual distance is acquired via the HC-SR04 ultrasonic sensor
$d_{j,o_{,min}}$	The theoretical minimum distance value
γ	The internal state variable
$\hat{E}$	The estimated lumped disturbance
G	Observer gain
$\hat{C}$	Estimated centrifugal force matrix
$\hat{G}$	Nominal gravity torque vector
$\hat{M}$	Nominal inertia matrix
$\tilde{E}$	The lumped uncertainty term
λ_a	Disturbance compensation adjustment coefficient
g_{rp}	Reference desired trajectory
$\hat{\varphi}$	Adaptive law parameter
κ	The derivative of the RITSMC function

1. Introduction

The continuum flexible robotic arm, as a novel robotic structure devoid of rigid joints and capable of continuous deformation, derives its core advantage from its ability to mimic flexible motion patterns such as the human spine [1, 2]. This enables it to operate in narrow, unstructured, and complex workspaces inaccessible to traditional rigid robots, positioning it as a key alternative to rigid robots in specialized scenarios. The discrete joint control paradigm of conventional rigid robots cannot effectively accommodate the demands of continuous flexible deformation, rendering the dynamic characteristic analysis and trajectory stability control of slender flexible manipulators critical determinants of operational precision and safety [3]. Consequently, related research has emerged as a prominent focus in the field of robotics. Current research on continuum flexible manipulators centers on dynamic modeling, trajectory planning, and high-precision control, forming a research landscape characterized by the integration of multiple methodologies. However, under the demanding conditions of industrial scenarios, traditional Model Predictive

Control (MPC) fails to simultaneously meet the application requirements for real-time performance, feasibility, and safety. Currently, researchers have initiated various improvements and optimizations to further enhance the trajectory replanning and tracking performance of MPC in the presence of obstacles. Representative studies are as follows: Kim et al. [4] developed a Gaussian Observer-based Model Predictive Control (GO-MPC) for path replanning under dynamic obstacle avoidance. This work makes a valuable contribution by integrating a Gaussian observer into the MPC framework to estimate the motion state of obstacles, thereby ensuring the generation of collision-free paths in dynamic environments. The significance of this study lies in its ability to handle uncertain obstacle information, which provides an effective solution for safe navigation of robots in complex dynamic scenarios. Li et al. [5] designed an adaptive Artificial Potential Field-based MPC (APF-MPC) avoidance strategy for dynamic obstacles. This research is notable for combining the computational efficiency of APF with the predictive capability of MPC, leveraging the iterative operation of MPC to predict obstacle trajectories. This work improved real-time performance and adaptability to dynamic environments, offering a practical approach for real-time obstacle avoidance control. Ning et al. [6] proposed a recursive sliding mode control (RSMC) scheme that improves control accuracy while maintaining a simple control structure. This study makes an important contribution to the simplification of SMC design, achieving a favorable balance between control performance and structural complexity, which is of great significance for engineering applications. Alsaied et al. [7] proved that the application of Integral Sliding Mode Control (ISMC) to trajectory tracking control could enhance convergence speed by eliminating the reaching phase. This finding is of considerable theoretical value as it reveals that removing the reaching phase can effectively improve the transient performance of SMC systems, providing a new perspective for the design of high-performance sliding mode controllers. Nevertheless, conventional ISMC generally relies on linear sliding functions and can only achieve asymptotic convergence, which limits its ability to achieve finite-time control precision. Silva et al. [8] developed the Fast Non-Singular Terminal Sliding Mode Control (FNTSMC). This work represents a significant advancement in terminal sliding mode control theory by successfully avoiding the singularity problem while realizing finite-time convergence. Meanwhile, the adoption of the sign function easily causes severe chattering, and complex disturbance issues remain unresolved, which are critical challenges that need to be addressed for practical implementation. Ramalingam et al. [9] designed an output error-based feedback controller, where the error is defined as the difference between the sensor-measured output and the reference variable. This study provides valuable insights into the design of output feedback control for systems with sensor uncertainties, offering an effective optimization-based approach for improving control performance under measurement constraints. Efafi et al. [10] addressed the issues of joint elasticity, parameter uncertainty, and external disturbances by proposing to incorporate fractional-order calculus theory into the Extended State Observer (ESO) design. This work makes a notable contribution to the field of state estimation for flexible systems by leveraging the memory and non-local properties of fractional-order operators to enhance estimation accuracy. In addition to ESO-based approaches, Nonlinear Disturbance Observers (NDOs) have also been widely investigated for disturbance rejection in various robotic and mechatronic systems. For instance, a nonlinear disturbance observer-based super-twisting sliding mode controller was developed for knee-assisted exoskeleton robots, which combines the disturbance estimation capability of NDO with the robustness of second-order sliding mode control to achieve precise trajectory tracking under external disturbances [11]. For electronic throttle valve systems, an active unmatched disturbance rejection quasi-sliding observer was proposed based on backstepping control, which effectively handles unmatched disturbances through the quasi-sliding mode observation mechanism [12]. Furthermore, a Backstepping-Based Nonlinear Disturbance Observer (BS-NLO) was designed for speed control of DC motors, leveraging the backstepping framework to deal with unmatched disturbances while ensuring system stability [13].

Despite the effectiveness of these NDO-based methods in their respective application domains,

they often require accurate model information for observer design and may exhibit limited adaptability to time-varying and multi-source disturbances in complex flexible systems. Moreover, most existing disturbance observers are designed for specific rigid systems and lack targeted consideration of the rigid-flexible coupling characteristics and multi-source disturbance characteristics of flexible manipulators.

Despite the significant progress achieved by current research, several key limitations remain to be addressed for trajectory tracking and vibration control of flexible manipulators in complex dynamic environments. Existing MPC-based path planning methods primarily focus on obstacle avoidance for rigid robotic systems and suffer from high computational complexity, limiting real-time performance. Observer-based approaches have improved state estimation accuracy, but lack a hierarchical disturbance suppression mechanism that systematically compensates for model uncertainties, external disturbances, and flexible coupling perturbations in the control loop. Most importantly, there is a lack of a unified framework that simultaneously addresses dynamic obstacle avoidance, trajectory optimization, vibration suppression, and disturbance rejection for flexible manipulators, and the performance boundaries of different strategies under various operating conditions remain insufficiently clarified. To address these limitations, this study proposes a comprehensive control scheme combining STO-MPC trajectory replanning and ADO-RITSMC cooperative vibration suppression for flexible manipulators, aiming to provide a systematic solution for achieving safe, precise, and stable operation of flexible robots in dynamic environments where conventional methods fail to simultaneously satisfy the requirements of real-time obstacle avoidance, trajectory accuracy, vibration suppression, and robust stability. Compared with previous studies, the main innovation points of this study are as follows:

(1) Combined with the motion characteristics of flexible manipulators, a real-time STO-MPC trajectory replanning framework was constructed. By integrating stochastic trajectory optimization and receding horizon mechanisms of model predictive control, probabilistic obstacle avoidance constraints and gradient-independent solving methods were introduced. The requirements of structural stiffness restriction and residual vibration suppression for flexible structures were satisfied, while the computational cost of the algorithm was effectively reduced, and the defects of poor dynamic adaptability and high solution delay existing in traditional global planning methods were addressed.

(2) A cooperative vibration suppression strategy integrating ADO and RITSMC was proposed. Model-free real-time compensation for model uncertainties, external disturbances and flexible coupling perturbations was realized by the adaptive disturbance observer. Combined with the finite-time convergence performance of non-singular terminal sliding modes, control outputs were optimized. The inherent chattering problem of conventional sliding mode control was fundamentally weakened, a hierarchical disturbance suppression mechanism was formed, and the dynamic stability of the flexible system was enhanced.

(3) A multi-condition comparative verification system was established. O-shaped continuous trajectories and V-shaped high-curvature trajectories were selected as typical test paths, and GO-MPC, APF-MPC and traditional sliding mode algorithms were adopted for comparative experiments. Algorithm performances were quantitatively evaluated from multiple dimensions including computational efficiency, state estimation accuracy, trajectory fitting degree and vibration suppression capability. The applicable boundaries of different planning and control methods were clarified, and sufficient experimental references were provided for the scheme selection of dynamic obstacle avoidance control of flexible manipulators.

Compared with existing manipulators and conventional control algorithms including GO-MPC, APF-MPC and FNTSMC, the proposed continuum flexible manipulator together with the combined STO-MPC and ADO-RITSMC framework achieves prominent overall advantages: the gradient-free STO-MPC planner removes heavy computational burden from gradient-based solvers and implements real-time mid-run trajectory adjustment without halting manipulator movement, and the probabilistic obstacle-avoidance constraints as well as stiffness-related limits fully account for intrinsic flexible-structure characteristics ignored by traditional

rigid-robot-oriented MPC methods; the ADO-RITSMC controller realizes model-free compensation of multi-source disturbances and finite-time error convergence, suppresses chattering and residual vibration by 16.7 % and attains over-90 % disturbance rejection rate, which overcomes the drawbacks of serious chattering and only asymptotic convergence existing in conventional sliding-mode controllers. Testing under O-shaped continuous trajectories validates its stable tracking performance for routine continuous-motion tasks, while high-curvature V-shaped trajectories verify its reliability under sharp-turn-induced strong rigid-flexible coupling, which represents practical working conditions in narrow-space industrial assembly, part sorting and confined-environment machining scenarios; the satisfactory real-time performance, low vibration and high tracking accuracy also extend its application potential to medical minimally-invasive operation and automated pipeline inspection, and the comparative experiments clarify applicable boundaries of different algorithms to offer practical references for engineers selecting planning and control schemes for flexible-manipulator-oriented industrial equipment.

2. Construction of dynamic characteristic analysis model

2.1. Composition and motion description of robots

As shown in Fig. 1(a), the flexible manipulator investigated in this paper is a type of continuum robot, whose core principle lies in realizing complex spatial movements by driving the continuous flexible backbone to generate controllable bending deformation through the coordinated motion of actuation units (e.g., cables, springs or push rods). Among its components, the flexible backbone serves as the main support of the manipulator, and it is composed of multiple serially connected joint disks and elastic elements, enabling bending and torsion in multiple directions [14, 15]. The stainless steel spring provides axial elastic support to maintain the overall stiffness of the manipulator while allowing bending deformation. The cable actuation system exerts tensile forces on joint disks at different positions by controlling the length variation of multiple cables, thereby driving the manipulator to produce movements such as bending and torsion. The joint disks are evenly distributed on the flexible backbone, which are used to fix the cables and springs, transmit driving forces, and ensure the continuity and smoothness of deformation [16-18].

The flexible manipulator has two primary degrees of freedom, including bending and torsion. The pose state of the flexible manipulator can be achieved by adjusting the spatial bending angle θ and rotation angle α. For the convenience of expression, the corresponding workspace position vector is denoted as $w = [x, y, z]^T$, and the joint space configuration vector is denoted as $h = [\theta, \alpha]^T$. The kinematics of the manipulator can be expressed as follows:

$$w = p(h) = \left[\frac{d}{\theta}\cos\alpha(1-\cos\theta) \quad \frac{d}{\theta}\sin\alpha(1-\cos\theta) \quad \frac{d}{\theta}\sin\theta\right]^T. \tag{1}$$

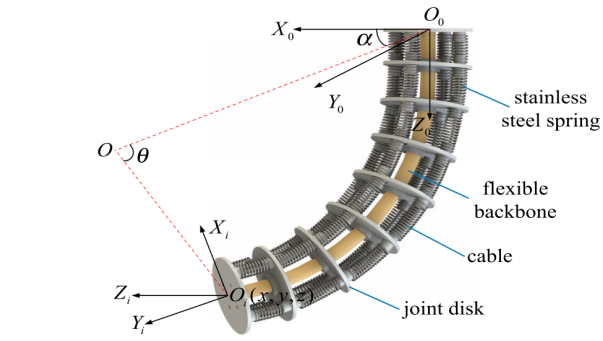
According to the pose control principle shown in Fig. 1(b), the curvature radius of the driving rope can be represented as:

$$\zeta_i = \zeta - r\cos\alpha_i, \tag{2}$$

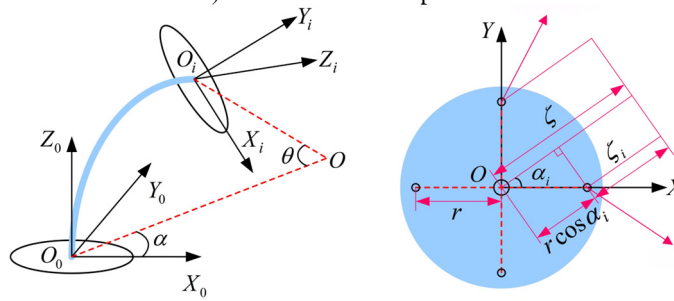
where ζ represents the curvature radius measured from the center of the disc, ζ_i represents the bending curvature radius of the i-th driving rope, r represents the distance between the center of the disc and the center of each routing hole, and α_i represents the rotation angle of the i-th driving rope.

The relationship between the length variation of the drive rope and the bending angle of the drive rope is:

$$\Delta l_i = (\zeta - \zeta_i)\theta = r\theta\cos\alpha_i. \tag{3}$$



a) Main structural components



b) Principle of pose control

Fig. 1. Composition and control principle of flexible robotic arm

According to the Lagrangian method, the dynamic equation of the robotic arm can be expressed as:

$$Q(h)\ddot{h} + F(h,\dot{h})\dot{h} + E(h) + \psi_f = \psi, \tag{4}$$

where Q is the inertia matrix, F is the matrix of Coriolis force and centrifugal force, which describes the Coriolis force and centrifugal force generated during the motion of the robotic arm. These forces vary with the joint velocity and are particularly significant during high-speed motion. E is the vector of gravity term, which describes the heavy moment or gravity experienced by each link of the robotic arm in the gravity field, and is a key term for maintaining the static balance of the robotic arm.ψ_f represents the flexible effect vector, which is a term unique to flexible robotic arms and includes damping and restoring forces caused by link elastic deformation and joint flexible vibration. ψ is the generalized force input vector, representing the driving torque applied to the joints of the robotic arm, and is the input that drives the motion of the robotic arm.

In order to facilitate robust control, adaptive control, and model uncertainty analysis, the dynamic equations of the flexible robotic arm will be subjected to nominal error decomposition, and the key terms can be expressed as:

$$\begin{cases} Q(h) = \hat{Q}(h) + \Delta Q(h), \\ F(h,\dot{h}) = \hat{F}(h,\dot{h}) + \Delta F(h,\dot{h}), \\ E(h) = \hat{E}(h) + \Delta E(h), \end{cases} \tag{5}$$

where the items before and after the plus sign represent the nominal matrix and error matrix of the actual matrix, respectively. Thus, Eq. (4) can be further formulated as:

$$\hat{Q}(h)\ddot{h} + \hat{F}(h,\dot{h})\dot{h} + \hat{E}(h) = \psi - X(h,\dot{h},\ddot{h}). \tag{6}$$

$X(h,\dot{h},\ddot{h})$ is the systematic error term, which can be defined as:

$$X(h,\dot{h},\ddot{h}) = \psi_f + \Delta Q(h)\ddot{h} + \Delta F(h,\dot{h})\dot{h} + \Delta E(h). \tag{7}$$

Considering the error between the set trajectory and the actual trajectory of the robotic arm, the formula can be expressed as:

$$\hat{Q}(h)\ddot{e} = \psi - X(h,\dot{h},\ddot{h}) - \hat{F}(h,\dot{h})\dot{h} - \hat{E}(h) - \hat{Q}(h)\ddot{h}_d, \tag{8}$$

where h_d stands for the desired position vector, e represents the trajectory error matrix.

2.2. Design of STO-MPC trajectory replanning

It is necessary to obtain the position and speed of obstacles since the obstacles are dynamic, which is a critical prerequisite for the safe and effective operation of the STO-MPC trajectory replanning algorithm for flexible manipulators. If the speed of the jth obstacle is set to V_{oj}, then its motion equation can be expressed as:

$$\begin{aligned} w_{o_j}(k+1) &= w_{o_j}(k) + TV_{o_j}(k), \\ V_{o_j}(k+1) &= V_{o_j}(k) + T\xi_{o_j}(k), \end{aligned} \tag{9}$$

where $V_{oj}(k)$ and ζ_{oj} represent the nearest distance from the jth obstacle to the end-effector and the velocity variation rate of the jth obstacle, respectively.

The schematic diagram of STO-MPC trajectory replanning for a flexible manipulator is shown in Fig. 2. Initially, the flexible manipulator follows a pre-planned desired trajectory from the start point to the end point. When a dynamic obstacle appears in the workspace and poses a collision threat to the original trajectory, the STO-MPC algorithm immediately triggers trajectory replanning. This process utilizes real-time obstacle position and velocity information obtained from sensing devices. During replanning, the algorithm takes into account both the dynamic constraints of the flexible manipulator's links (such as residual vibration suppression and stiffness limits) and the collision avoidance constraints imposed by dynamic obstacles. It then generates a new trajectory that bypasses the obstacles, ultimately ensuring that the flexible manipulator reaches the end point from the start point safely and stably. This clearly demonstrates the algorithm's core technical features of real-time optimization and reactive obstacle avoidance, highlighting its critical role in enabling the flexible manipulator to perform tasks safely and efficiently in dynamic environment.

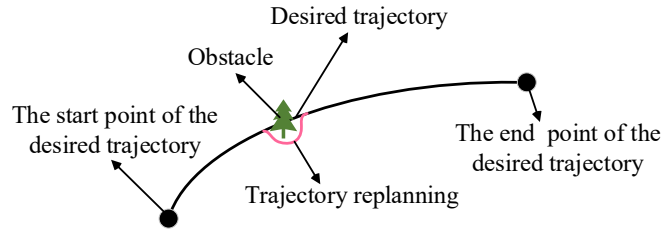


Fig. 2. Schematic diagram of path planning

To guarantee safety during obstacle avoidance, constraint conditions for trajectory tracking need to be defined. A cost function is introduced to maintain a safe distance between the flexible manipulator and the j-th obstacle, which can be formulated as follows:

$$O_{o,j} = \frac{A_o}{d_{j,o}^2 + \sigma}, \tag{10}$$

where A_o is the weight coefficient, $d_{j,o}$ is the distance between the flexible manipulator and the j-th obstacle. σ is a small positive number that guarantees the flexible manipulator is not zero.

To avoid singularities during optimization and mitigate the impact of insignificant distance fluctuations on the adjustment of the cost function, the value of σ is selected as 0.06. The constraints of the safe distance between the flexible manipulator and obstacles can be defined as:

$$O_{o,j}^* = \begin{cases} \dfrac{A_o}{{d_{j,o}^*}^2 + 0.06}, & d_{j,o}^* \le d_{j,o_{,min}}, \\ 0, & \text{otherwise}, \end{cases} \tag{11}$$

where $d_{j,o}^*$ is the actual distance is acquired via the HC-SR04 ultrasonic sensor, $d_{j,o_{,min}}$ is the theoretical minimum distance value.

The STO-MPC trajectory replanning system imposes high demands on both hardware and software, with its core objective being the construction of a closed-loop computing platform capable of real-time perception, rapid optimization, and precise control. At the hardware level, the system relies on heterogeneous high-performance computing units composed of multi-core CPUs and FPGAs/GPUs to handle complex model predictive control algorithms. It must also be equipped with high-frame-rate vision sensors and high-precision encoders to capture the real-time status of dynamic obstacles and the flexible links. All data streams must be strictly time-synchronized via real-time industrial Ethernet buses. At the software level, the system must run on a real-time operating system to ensure deterministic scheduling. It requires the integration of efficient embedded numerical optimization solvers to complete constrained trajectory replanning within milliseconds. Additionally, it must incorporate accurate dynamic models and multi-sensor data processing algorithms to achieve full logical integration from state estimation and obstacle perception to obstacle avoidance trajectory generation. This ensures the safety and stability of the flexible manipulator when operating in dynamic and unstructured environments. To improve trajectory optimization and model prediction performance, probabilistic obstacle avoidance constraints and gradient independent solving methods can be introduced.

(1) Probabilistic obstacle avoidance constraints.

Traditional MPC planners adopt fixed hard distance limits to avoid collisions between the manipulator and obstacles, which cannot accommodate random motion noise of dynamic obstacles. If the preset safety margin is too small, unexpected collisions may occur due to obstacle position fluctuations. If the margin is excessively large, the generated trajectory will be overly conservative and severely restrict the movement space of the flexible manipulator. The probabilistic constraint design can automatically adjust the safety buffer distance according to the real-time motion uncertainty of obstacles. When obstacles move steadily with tiny position noise, the planner retains a small safety gap to ensure flexible movement. When obstacles exhibit drastic and unstable motion, the system automatically expands the separation distance to reduce collision risks. Meanwhile, two additional constraint rules are embedded into the optimization framework: one limits the maximum bending curvature of the flexible backbone to protect the elastic structure from excessive deformation damage, and the other restrains the end-effector acceleration amplitude to suppress residual vibration of flexible links. All these soft and hard constraints work together to balance obstacle avoidance safety, structural stiffness limits and vibration suppression demands.

(2) Gradient-independent solving mechanism.

The optimization objective of STO-MPC involves highly nonlinear rigid-flexible coupling dynamics of the continuum manipulator and non-smooth probabilistic obstacle avoidance constraints. If conventional gradient-based optimization solvers are applied, the objective function

and constraint equations will produce unstable, vanishing or oscillating gradient values during each iterative solution. Repeated gradient derivation and matrix inversion bring heavy computational burden, leading to obvious calculation delay and poor real-time performance, which cannot meet the high-frequency control requirement of flexible manipulators. For this reason, a gradient-independent sampling solution strategy is adopted in the STO-MPC framework, which completely removes the reliance on gradient information of both cost function and constraint conditions. At each rolling optimization step, the algorithm generates a batch of candidate control sequences via Gaussian random sampling around the nominal control input. Each candidate control sequence is imported into the flexible manipulator dynamic model to predict the complete trajectory within the prediction horizon. The sampling range can be adjusted offline by tuning the covariance of random Gaussian noise to balance solving speed and trajectory optimization quality. This gradient-free mechanism eliminates the numerical computation overhead of gradient-related operations, cuts down single-cycle solving time remarkably, and fundamentally overcomes the long computation delay and weak dynamic adaptability defects of traditional global trajectory planning algorithms.

2.3. Design of ADO-RITSMC trajectory

Aiming at the core challenges faced by flexible continuum manipulators in performing high-precision tasks in dynamic obstacle environments, including model uncertainties, residual vibration of flexible links, external disturbances, and real-time threats from dynamic obstacles, the design of the ADO-RITSMC trajectory control scheme establishes a trajectory tracking and obstacle avoidance control framework with strong robustness, finite-time convergence, and real-time disturbance rejection capability, as shown in Fig. 3. The ADO is adopted to estimate and compensate in real time for the internal uncertainties of the system (such as elastic deformation and parameter perturbations of flexible links) and external disturbances, thereby fundamentally reducing the impact of disturbances on trajectory tracking accuracy. On this basis, RITSMC is constructed: an integral term is introduced to eliminate steady-state errors, the finite-time convergence property of terminal sliding mode is utilized to improve dynamic response speed, and robust terms are applied to suppress observer residual errors and unmodeled dynamics, which significantly alleviates the chattering problem in conventional sliding mode control. At the trajectory level, the design process deeply integrates key constraints such as the closest position and velocity rate change of dynamic obstacles (e.g., the closest position of the j-th obstacle relative to the end-effector and its rate change of velocity as mentioned above) with the ADO-RITSMC control law, achieving collaborative optimization of trajectory tracking accuracy, disturbance rejection performance, and real-time obstacle avoidance safety. Ultimately, this scheme can provide stable and reliable underlying control support for the STO-MPC (Stochastic Trajectory Optimization-Model Predictive Control) trajectory replanning algorithm, ensuring that the flexible manipulator accomplishes high-precision operational tasks safely and efficiently in complex dynamic environments.

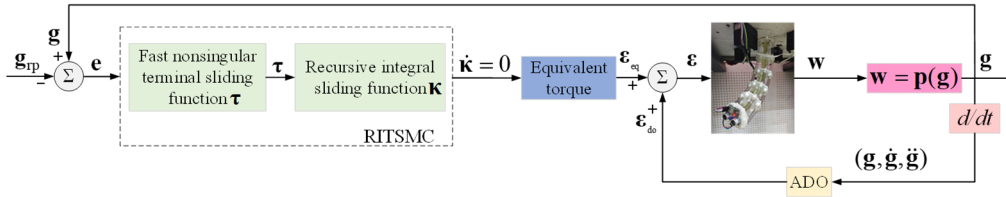


Fig. 3. The ADO-RITSMC trajectory control scheme

Based on the closed-loop control architecture described above, the operational logic of the ADO-RITSMC trajectory control scheme during dynamic obstacle avoidance of a flexible manipulator forms a complete closed-loop iterative process. When the upper-level STO-MPC

algorithm generates a new desired trajectory based on the real-time status of dynamic obstacles, the system first calculates the tracking error between the desired trajectory and the actual position of the end-effector, which is then fed into the RITSMC core module. This module, through the synergy of a fast nonsingular terminal sliding mode function and a recursive integral sliding mode function, rapidly computes the equivalent control torque under disturbance-free conditions. Simultaneously, based on the real-time pose, velocity, and acceleration information of the end-effector, the ADO module accurately estimates the lumped disturbances, including elastic deformation of the flexible links, parameter perturbations, and disturbances from dynamic obstacles, and outputs a disturbance compensation term. During the control command synthesis stage, the system integrates the equivalent torque with the disturbance compensation term to generate the actual disturbance-rejection control torque, which is then applied to the joint drive units of the flexible manipulator. After the manipulator executes the control command, the actual motion of its end-effector is transformed into feedback signals via pose mapping. These signals are, on one hand, sent back to the error calculation module to update the trajectory tracking error and, on the other hand, continuously fed into the ADO module to enable real-time iteration of disturbance estimation. This closed-loop iterative mechanism ensures that the ADO-RITSMC control scheme can, during the process of the flexible manipulator following the STO-MPC replanned trajectory, mitigate the adverse effects of model uncertainties and external disturbances in real time, effectively suppress the residual vibration of the flexible links, and maintain high-precision trajectory tracking performance of the end-effector in dynamic obstacle environments.

ADO can effectively provide compensation calculations for control inputs while estimating interference. The disturbance observer can be represented as [19]:

$$\begin{aligned}&\dot{\gamma} = -G\hat{E}(g,\dot{g},\ddot{g}) + G\left(\varepsilon - \hat{C}(g,\dot{g})\dot{g} - \hat{G}(g)\right),\\&\hat{E}(g,\dot{g},\ddot{g}) = \gamma - G\widehat{M}(g)\dot{g},\end{aligned} \tag{12}$$

where γ is the internal state variable, g is joint position vector, $\hat{E}$ represents the estimated lumped disturbance, G is observer gain, $\hat{C}$ is estimated centrifugal force matrix, $\hat{G}$ is nominal gravity torque vector, $\widehat{M}$ is nominal inertia matrix.

The derivative can be represented as:

$$\begin{aligned}\dot{\tilde{E}}(g,\dot{g},\ddot{g}) &= \dot{\hat{E}}(g,\dot{g},\ddot{g}) - \dot{E}(g,\dot{g},\ddot{g})\\&= -G\hat{E}(g,\dot{g},\ddot{g}) + G\left(\varepsilon - \widehat{M}(g)\ddot{g} - \hat{C}(g,\dot{g})\dot{g} - \hat{G}(g)\right) - \dot{E}(g,\dot{g},\ddot{g})\\&= -G\hat{E}(g,\dot{g},\ddot{g}) + GE(g,\dot{g},\ddot{g}) - \dot{E}(g,\dot{g},\ddot{g}) = -G\tilde{E}(g,\dot{g},\ddot{g}) - \dot{E}(g,\dot{g},\ddot{g}),\end{aligned} \tag{13}$$

where $\tilde{E}$ stands for the lumped uncertainty term composed of system model errors, external disturbances and unmodeled dynamics.

In order to enhance the anti-interference ability, an adaptive law is adopted to compensate for the control input as followed [20]:

$$\varepsilon_{do} = \psi\left(g, g_{rp}, \dot{g}, \dot{g}_{rp}\right)\hat{\varphi} - \lambda_a\tilde{E}(g,\dot{g},\ddot{g}), \tag{14}$$

where λ_a is disturbance compensation adjustment coefficient, g_{rp} stands for reference desired trajectory, $\hat{\varphi}$ is adaptive law parameter, which can be expressed as:

$$\dot{\hat{\varphi}} = -\delta\left|\psi^T\left(g, g_{rp}, \dot{g}, \dot{g}_{rp}\right)\tilde{E}(g,\dot{g},\ddot{g})\right|, \tag{15}$$

where δ is adaptive step size coefficient.

From an engineering application perspective, this design overcomes the technical bottlenecks

of traditional sliding mode control in flexible manipulator applications, such as significant chattering and substantial steady-state errors. It also addresses the limitations of standalone active disturbance rejection control in achieving rapid dynamic response. Through the deep integration of ADO and RITSMC, the flexible manipulator can not only swiftly adjust its motion state in response to sudden positional changes of dynamic obstacles, leveraging the finite-time convergence characteristics of RITSMC, but also maintain control stability by relying on the real-time disturbance compensation capability of ADO. Ultimately, this achieves cross-level synergy, providing core technical support for the large-scale application of flexible manipulators in high-precision dynamic operation scenarios such as industrial assembly and minimally invasive medical surgery.

To ensure the reliability of the ADO-RITSMC trajectory control scheme, stability analysis can be conducted based on Lyupunov's theorem. The Lyapunov function V_T can be constructed as:

$$V_T = \frac{1}{2}\kappa^2 + \frac{1}{2}\delta^{-1}\hat{\varphi}^2, \tag{16}$$

where κ is the derivative of the RITSMC function.

By combining Eq. (12) and Eq. (14), the derivative of Eq. (16) can be expressed as:

$$\begin{aligned}\dot{V}_T &= \kappa\dot{\kappa} + \hat{\varphi}\delta^{-1}\dot{\hat{\varphi}} = \kappa\frac{\varepsilon}{\widehat{M}(g)} - \hat{\varphi}\delta^{-1}\delta\left|\psi^T\left(g, g_{rp}, \dot{g}, \dot{g}_{rp}\right)\tilde{E}(g, \dot{g}, \ddot{g})\right| \\ &= \kappa\frac{1}{\widehat{M}(g)}\varepsilon - \hat{\varphi}\left|\psi^T\left(g, g_{rp}, \dot{g}, \dot{g}_{rp}\right)\tilde{E}(g, \dot{g}, \ddot{g})\right| \\ &= -\kappa\frac{1}{\widehat{M}(g)}\left(\lambda_a\tilde{E}(g, \dot{g}, \ddot{g}) - \psi\left(g, g_{rp}, \dot{g}, \dot{g}_{rp}\right)\hat{\varphi}\right) - \hat{\varphi}\left|\psi^T\left(g, g_{rp}, \dot{g}, \dot{g}_{rp}\right)\tilde{E}(g, \dot{g}, \ddot{g})\right| \\ &= -|\kappa|\frac{1}{\widehat{M}(g)}\left(\lambda_a\tilde{E}(g, \dot{g}, \ddot{g}) - \psi\left(g, g_{rp}, \dot{g}, \dot{g}_{rp}\right)\hat{\varphi}\right) - |\hat{\varphi}|\left|\psi^T\left(g, g_{rp}, \dot{g}, \dot{g}_{rp}\right)\tilde{E}(g, \dot{g}, \ddot{g})\right|,\end{aligned} \tag{17}$$

where ε is the lumped error term obtained after expanding the sliding mode dynamics.

For convenience of expression, define parameters L_1 and L_2 as:

$$\begin{aligned}L_1 &= \frac{1}{\widehat{M}(g)}\left(\lambda_a\tilde{E}(g, \dot{g}, \ddot{g}) - \psi\left(g, g_{rp}, \dot{g}, \dot{g}_{rp}\right)\hat{\varphi}\right), \\ L_2 &= \left|\psi^T(g, g_{rp}, \dot{g}, \dot{g}_{rp})\tilde{E}(g, \dot{g}, \ddot{g})\right|.\end{aligned} \tag{18}$$

Eq. (14) can be expressed in another form as followed:

$$\dot{V}_T \le -\left[L_1\sqrt{2}\frac{|\kappa|}{\sqrt{2}} + \frac{L_2\sqrt{2}}{\sqrt{\delta^{-1}}}\frac{\sqrt{\delta^{-1}}}{\sqrt{2}}|\hat{\varphi}|\right] \le -R\left(\frac{|\kappa|}{\sqrt{2}} + \frac{\sqrt{\delta^{-1}}}{\sqrt{2}}|\hat{\varphi}|\right) = -RV_T^{\frac{1}{2}}. \tag{19}$$

According to Eq. (19), it is confirmed that $L_1 > 0$ and $L_2 > 0$, which implies $R > 0$. Hence, this completes the stability proof.

2.4. Overall design of motion control and obstacle avoidance schemes

To effectively achieve the functions of obstacle perception, trajectory replanning, and adaptive robust tracking control of the flexible robotic arm, the control process is designed as shown in Fig. 4. The left module is mainly used for environment perception and trajectory replanning. It employs the STO (Super-Twisting Observer), a super-twisting obstacle and state observer, to achieve robust estimation of dynamic obstacles and the robot's own state. As a type of second-order sliding mode observer, the super-twisting observer introduces an integral term,

which not only maintains the finite-time convergence characteristic but also significantly mitigates the chattering problem inherent in traditional sliding mode observers. It extracts dynamic information of obstacles and estimates the robot's own motion state from the motion state feedback and control inputs of the robotic arm.

This control scheme offers notable advantages: for example, it is more adaptable to complex dynamic environments than the Kalman filter, and it provides higher estimation accuracy and less chattering than first-order sliding mode observers, thereby delivering more reliable environmental perception data for subsequent planning. Even when sensors are affected by noise, delays, or measurement errors, it can still output reliable obstacle and state estimates, providing accurate environmental information for subsequent planning. The core function of MPC Trajectory Replanning is to dynamically generate obstacle-avoiding trajectories based on receding horizon optimization. MPC solves a finite-time-horizon optimal control problem at each step through its rolling mechanism of prediction, optimization, and feedback. The replanning capability allows the trajectory to be adjusted in real time as obstacles move dynamically, avoiding the failure of traditional global planning in dynamic environments.

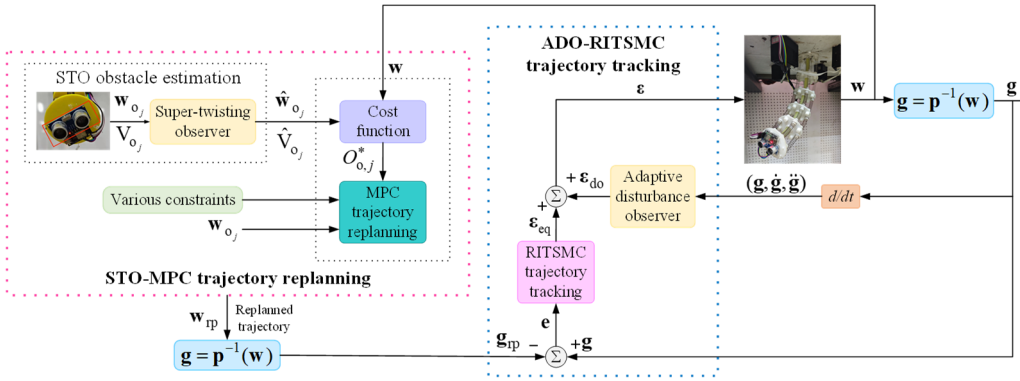


Fig. 4. Closed-loop control process of motion control and obstacle avoidance

STO-MPC (Stochastic Trajectory Optimization-Model Predictive Control) trajectory replanning is defined as a dynamic trajectory updating method integrated with stochastic trajectory optimization and model predictive control. On the basis of the system dynamic model, its core implementation process is as follows: an initial feasible trajectory is first generated by planners such as RRT. Then candidate trajectories with Gaussian noise are generated under a preset covariance matrix with the sampling time as the step size, which is usually set as 1/20 to 1/10 of the system open-loop response time. After being evaluated and screened by the cost function, the trajectory is updated via receding horizon optimization, and only the first control input within the 2-5 steps of the control horizon is implemented. Meanwhile, hard constraints are converted into probabilistic constraints with a confidence level of 95 %-99 %, and closed-loop feedback correction is achieved with an online replanning frequency of 10-100 Hz, thus model errors and environmental disturbances are corrected. For this method, the prediction horizon is generally set to 1-5 s, and the control horizon accounts for 10 %-20 % of the prediction horizon. The gradient-free optimization mechanism is adopted to adapt to non-smooth constraints, and the computational cost is reduced via efficient trajectory parameterization. In addition, the balance between planning speed and trajectory quality can be achieved by adjusting the number of samples and iterations. This method is endowed with the advantages of strong robustness, high trajectory smoothness and multi-objective compatibility, and is compatible with both linear and nonlinear system models. The real-time computational load of sampling covariance can be reduced through offline approximation. It is widely applied to scenarios including dynamic obstacle avoidance of robotic arms, autonomous driving and UAV trajectory tracking, and the optimal collision-free trajectories that meet the amplitude limit requirements can be rapidly generated within 0.01-0.1 s.

The right module is designated as the core execution unit for high-precision control of flexible manipulators, and its core responsibilities are defined as the achievement of precise trajectory tracking of the end-effector, active suppression of multi-source disturbances, and stabilization of elastic vibrations in flexible links [21-23]. To address issues such as joint friction, elastic deformation of links, sudden load changes, and parameter perturbations, a collaborative architecture of ADO (Adaptive Disturbance Observer) and RITSMC is adopted, and a closed-loop logic for disturbance estimation, feedforward compensation, feedback stabilization, and vibration suppression is constructed.

This collaborative architecture is endowed with the technical advantages of both ADO and RITSMC, is adapted to the flexible manipulators, and exhibits strong engineering practicability. The model-free adaptive capability of ADO and the strong robustness of RITSMC are combined to generate a superposition effect. Through hierarchical disturbance processing (e.g., ADO is used to compensate for large global disturbances, and RITSMC is employed to suppress residual small disturbances), the requirement for sliding mode control gains is reduced, and elastic resonance induced by chattering is avoided. The architecture is designed with a modular structure: ADO can be independently embedded into the control loop, and RITSMC achieves collaborative control through an elastic vibration stabilization term. The overall computational complexity is linear, with a single-cycle time consumption ≤ 0.01 s, supporting high-frequency control above 100 Hz.

3. Testing and analysis of dynamic trajectory stability

3.1. Construction of the test platform

As shown in Fig. 5, the dynamic trajectory test platform for flexible manipulators is an experimental validation system built to verify high-precision trajectory tracking and real-time obstacle avoidance control algorithms (such as STO-MPC trajectory replanning and ADO-RITSMC low-level control) for cable-driven flexible continuum manipulators in environments with dynamic obstacles. The platform adopts a modular design and consists of four parts, including the flexible manipulator, the obstacle system, the multi-sensor perception system, and the control and drive system. The flexible manipulator features a segmented flexible spine as its core support, with internally embedded stainless steel springs to simulate elastic deformation. The springs are made of SUS301 stainless steel. After the flexible manipulator undergoes bending and torsional deformation, the springs can provide stable elastic restoring force to ensure reversible deformation of the arm. Meanwhile, stainless steel has high tensile strength, which enables it to withstand continuous reciprocating deformation and resist plastic deformation and rust during long-term operation. Thermoplastic Polyurethane (TPU) is adopted for the flexible central backbone. It combines the high flexibility of rubber and the favorable machinability of plastics, and possesses excellent bending and tear resistance. Serving as the central load-bearing skeleton of the continuum arm, TPU enables continuous and smooth bending to realize the continuum deformation of the manipulator. The joint disks are fabricated from engineering plastic (3D-printed ABS). The joint disks are mainly used for radial positioning, cable guiding and position restriction of the backbone, and primarily bear local compressive loads. Multifilament nylon is selected as the driving cable. Nylon wire features high tensile strength, small diameter and extremely low self-weight, with a smooth surface that produces low frictional resistance when passing through the guide holes of joints. The bending motion of the flexible arm is driven by servo motors pulling the cables. Since the cables are only subjected to uniaxial tension, the traction force can be transmitted efficiently. Cables are fixed to the joint disks and connected to the drive points of multiple high-precision servo motors, which control the manipulator's posture. The obstacle system includes fixedly installed static obstacles and dynamic obstacles mounted on moving sliders, capable of simulating static/dynamic obstacle threats. The perception system comprises an HC-SR04 ultrasonic sensor at the end-effector for obstacle distance information and a GY-95T attitude sensor for end-effector pose feedback. The control and drive system, through

servo drives, an embedded controller, and a high-speed communication module, enables real-time execution of algorithm commands and data interaction. The core function of the platform is to simulate complex dynamic operation scenarios, validating the tracking accuracy, stability, and obstacle avoidance capability of control algorithms under model uncertainties, external disturbances, and dynamic obstacles, while also supporting performance evaluation of multi-sensor fusion and cross-layer algorithm coordination.

All experiments are conducted in a controlled laboratory environment with a temperature of 25±2 °C and a relative humidity of 40 %-60 %, free from strong electromagnetic interference and mechanical vibration interference. The experimental platform is fixed on a marble optical platform to isolate ground vibration. The flexible manipulator has a total length of 600 mm, consisting of 12 serially connected aluminum alloy joint disks with a diameter of 30 mm. A stainless steel spring with a stiffness coefficient of 50 N/m is embedded in the center, providing a maximum bending angle of ±90° and a payload capacity of 0-5 kg. The drive system employs 4 Dynamixel MX-64T digital servo motors with a rated torque of 6 N·m, a position resolution of 0.088°, and a response time of ≤10 ms. The perception system includes an HC-SR04 ultrasonic sensor (measurement range: 2-400 cm, accuracy: ±3 mm), a GY-95T 9-axis IMU attitude sensor (gyroscope accuracy: ±0.05°/s, accelerometer accuracy: ±0.001 g, sampling frequency: 100 Hz), 12-bit absolute encoders, and a USB vision camera with a resolution of 1920×1080. The control system adopts an STM32F407 embedded controller with a main frequency of 168 MHz and a control frequency of 100 Hz. For the STO-MPC algorithm, the prediction horizon N is set to 10 and the control step Δt is set to 0.05 s. The sliding mode gain of RITSMC is set to 5.0, and the observer gain of ADO is set to 10. The obstacle system includes static obstacles with a diameter of 50 mm and dynamic obstacles mounted on a linear slider, with a maximum speed of 0.5 m/s and a positioning accuracy of ±0.1 mm. The effective workspace is 500 mm×500 mm×600 mm.

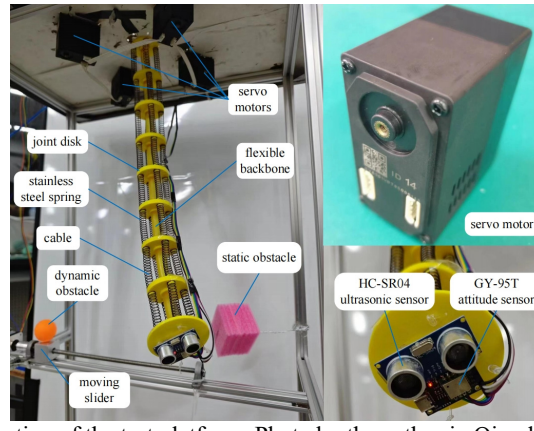


Fig. 5. The construction of the test platform. Photo by the author in Qingdao on March 1, 2026

3.2. Comparative analysis of accuracy in trajectory tracking

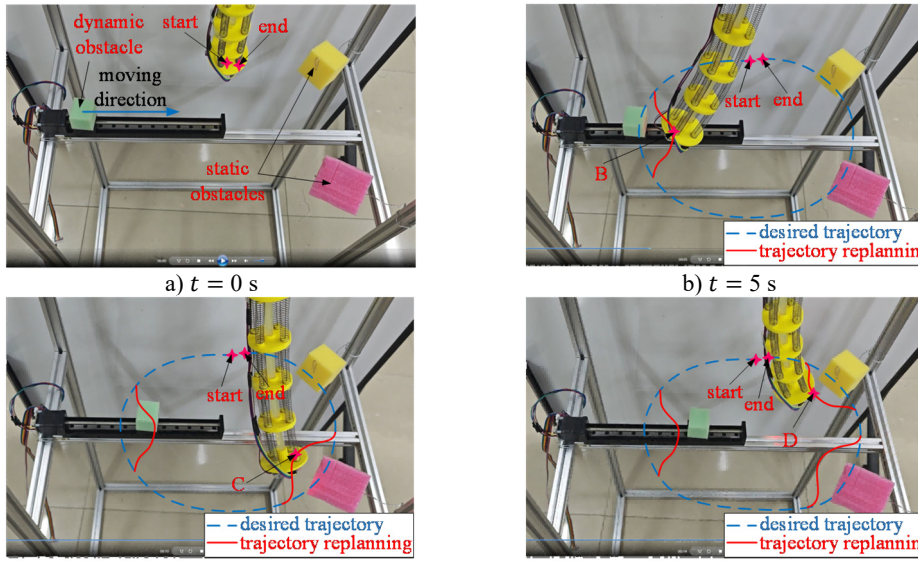
(1) Path Planning by STO-MPC.

The stochastic characteristic of the proposed STO-MPC is reflected in Gaussian random sampling for gradient-free optimization. The fluctuation range of sampling noise is constrained by a pre-calibrated covariance matrix to match the actual motion limits of the flexible manipulator joints, and a 95 % Gaussian confidence interval is adopted to balance the online calculation speed and the overall optimization quality of trajectories. After generating all candidate control sequences, the algorithm predicts the complete motion trajectory corresponding to each set of control signals based on the dynamic model of the flexible manipulator, calculates the comprehensive cost of each candidate trajectory, and selects the optimal trajectory as the

benchmark for the next cycle through weighted screening, which completely eliminates reliance on gradient-based solutions for complex nonlinear dynamics.

The optimization objective of STO-MPC calculates the overall deviation between the predicted joint motion trajectory and the preset ideal reference trajectory based on the evaluation component, which serves as the core indicator to guarantee the tracking accuracy of the end-effector. Meanwhile, the entire optimization process is subject to multiple physical constraints, including the upper and lower limits of the bending curvature of the flexible backbone determined by structural stiffness, the maximum operating speed of each joint, and the aforementioned statistical collision safety probability constraints.

The path planning results of STO-MPC are presented in Fig. 6. In this experiment, the path planning mechanism of STO-MPC is based on the framework of receding horizon optimization, and real-time trajectory replanning is achieved for the O-shaped trajectory tracking task of the flexible manipulator in an environment with both dynamic and static obstacles. The core logic is as follows: in each control cycle, based on the current state of the manipulator, the motion of the dynamic obstacle (e.g., uniform linear motion) within a finite time horizon is predicted by the algorithm, and an optimization problem incorporating obstacle avoidance safety distance constraints, trajectory tracking error costs, and control smoothness constraints is formulated in combination with the positions of static obstacles. After solving the control sequence, only the first control input is executed, and this process is repeated in the next cycle. When the dynamic obstacle enters the collision risk area of the reference trajectory, the local trajectory is forced to deviate from the reference path by adjusting the control input to achieve flexible obstacle avoidance, and a safe distance from the obstacles is maintained throughout the process to avoid collisions.



a) $t = 0$ s b) $t = 5$ s

c) $t = 10$ s d) $t = 14$ s

Fig. 6. Path planning results of STO-MPC. Photo by the author in Qingdao on March 5, 2026

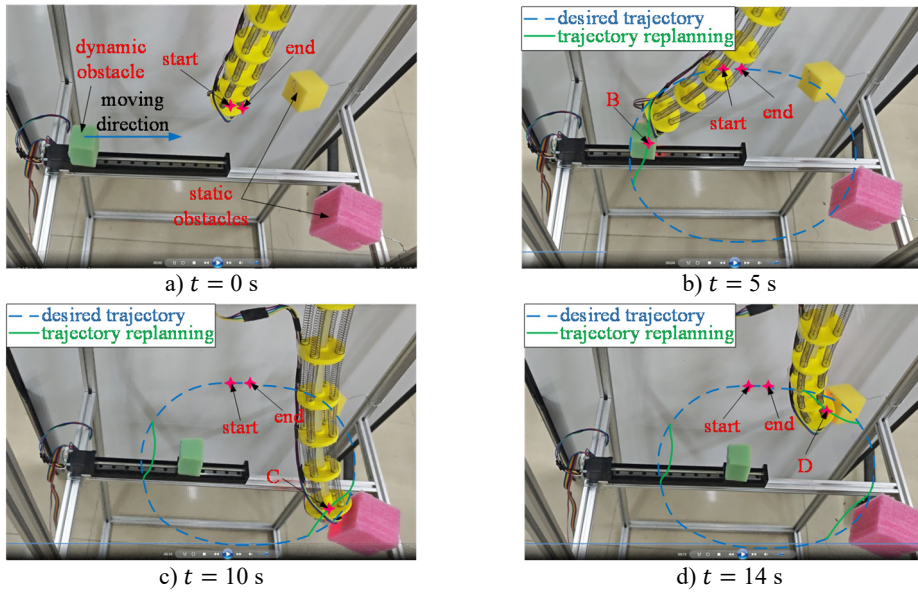
In terms of experimental performance, a balance between effective obstacle avoidance and trajectory tracking in dynamic environments is achieved by STO-MPC. When the dynamic obstacle approaches at $t = 5$ s, the manipulator actively adjusts its trajectory to the left to complete obstacle avoidance. When passing through the obstacle area at $t = 10$ s, a safe distance from the static obstacle is always maintained by the trajectory, and the motion is smooth without severe jitter. After the obstacle moves away at $t = 14$ s, the trajectory quickly returns to the reference path, and the O-shaped trajectory is finally completed. In the overall performance, the real-time

ISSN PRINT 1392-8716, ISSN ONLINE 2538-8460

performance and safety of dynamic obstacle avoidance are guaranteed by the algorithm, while high trajectory tracking accuracy is maintained in the undisturbed phase, demonstrating good adaptability and robustness to environments with mixed obstacles. The engineering feasibility of STO-MPC in the trajectory planning scenario of flexible manipulators is thus verified.

(2) Path Planning by GO-MPC.

The path planning results of GO-MPC are presented in Fig. 7. In this experiment, GO-MPC (Global Optimal Model Predictive Control) is adopted to implement trajectory replanning for the flexible manipulator in an environment with both dynamic and static obstacles. Its mechanism is based on a receding horizon optimization framework guided by global optimality. In each control cycle, with tracking the O-shaped reference trajectory as the global objective, the motion trajectory of the dynamic obstacle is predicted, and an optimization problem incorporating trajectory tracking error costs, obstacle avoidance safety distance constraints, and control smoothness constraints is formulated in combination with the positions of static obstacles. After the control sequence is solved, only the first control input is executed, and this process is repeated in the next cycle.



a) $t = 0$ s b) $t = 5$ s

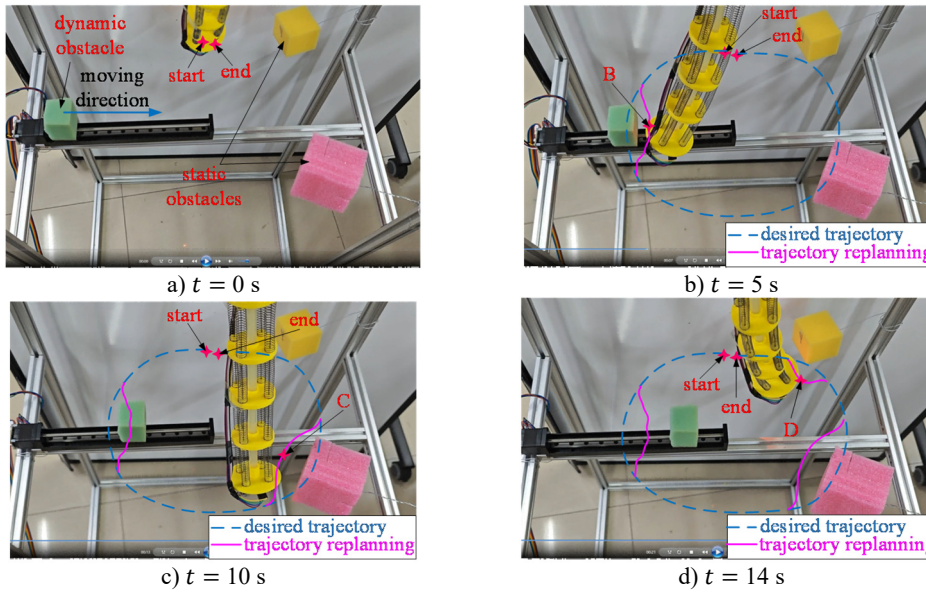
c) $t = 10$ s d) $t = 14$ s

Fig. 7. Path planning results of GO-MPC. Photo by the author in Qingdao on March 5, 2026

When the dynamic obstacle enters the collision risk area of the reference trajectory, a locally replanned trajectory is generated by adjusting the control input, prioritizing obstacle avoidance safety while maintaining consistency with the reference trajectory as much as possible, thus achieving real-time trajectory adjustment in dynamic environments. The experimental results demonstrate that GO-MPC exhibits excellent performance in balancing dynamic obstacle avoidance and trajectory tracking. At $t = 5$ s, when the dynamic obstacle approaches the reference trajectory, the manipulator avoids the obstacle in advance via the green replanned trajectory without collisions. At $t = 10$ s, the manipulator moves along the replanned trajectory, maintaining a safe distance from the static obstacle with smooth motion free of severe jitter. At $t = 15$ s, as the dynamic obstacle moves away, the manipulator's trajectory gradually returns to the reference path, and the complete O-shaped trajectory is finally accomplished. Overall, real-time avoidance of dynamic obstacles is achieved by the algorithm, while high trajectory tracking accuracy is maintained during obstacle avoidance, demonstrating good adaptability and robustness to environments with mixed obstacles. The engineering feasibility of GO-MPC in the trajectory planning scenario of flexible manipulators is thus verified.

(3) Path planning by APF-MPC.

The path planning results of APF-MPC are illustrated in Fig. 8. Based on the APF-MPC framework, trajectory replanning for flexible manipulators in mixed dynamic-static obstacle environments can be realized. By integrating the real-time obstacle guidance capability of the artificial potential field (APF) method with the receding horizon optimization of model predictive control (MPC), the hybrid control mechanism is constructed. Firstly, attractive potential fields are established to guide the manipulator to track reference trajectories and move toward target positions, while repulsive potential fields are generated to produce repulsive forces against dynamic and static obstacles for collision prevention. Subsequently, potential field guidance forces are converted into cost terms and constraint conditions of the MPC optimization problem. In each control cycle, the motions of dynamic obstacles are predicted according to the current system states, and the optimal control sequence that satisfies potential field guidance, obstacle avoidance constraints and control smoothness is solved. Only the initial control signal is executed before entering the next optimization iteration, thereby realizing real-time trajectory replanning combining potential field guidance and receding optimization. When dynamic obstacles approach the reference trajectory, the repulsive potential field drives the manipulator to deviate locally from the original path to complete flexible obstacle avoidance.



a) $t = 0$ s b) $t = 5$ s

c) $t = 10$ s d) $t = 14$ s

Fig. 8. Path planning results of APF-MPC. Photo by the author in Qingdao on March 5, 2026

Experimental results indicate that a favorable balance between obstacle avoidance and trajectory tracking in dynamic scenarios is achieved by APF-MPC. At $t = 7$ s, early obstacle avoidance is completed through the purple replanned trajectory under the action of repulsive potential fields as dynamic obstacles approach, and no collision occurs. At $t = 13$ s, the manipulator moves along the replanned path, where a stable safety distance from static obstacles is maintained and the overall trajectory remains smooth without violent vibration. At $t = 21$ s, the manipulator gradually returns to the reference path under the guidance of attractive potential fields after dynamic obstacles move away, and the complete tracking trajectory is ultimately finished. In general, rapid responses to dynamic obstacles are realized with the assistance of the real-time guidance characteristics of artificial potential fields, and trajectory smoothness as well as global task completion are guaranteed via MPC optimization. Satisfactory adaptability and robustness in mixed obstacle environments are demonstrated, which further validates the engineering applicability of APF-MPC for the trajectory planning of flexible manipulators.

The computational time of the three path planning algorithms is shown in Fig. 9 and Table 1. In terms of computational efficiency, distinct differences are observed among STO-MPC, GO-MPC and APF-MPC. The overall time consumption of STO-MPC is the lowest, with a peak value of only approximately 0.13 s, which rapidly converges to the range of 0-0.07 s. The optimal average efficiency is obtained, demonstrating that the simplified optimization framework is endowed with the highest real-time performance. The computational cost of GO-MPC falls in the middle, with a peak of about 0.14 s and a stable range of 0-0.08 s. Limited fluctuations are generated, and a desirable trade-off between efficiency and control performance is achieved. By comparison, significantly higher computational overhead is produced by APF-MPC. Its peak time exceeds 0.17 s, and periodic high-load operation occurs after 1 s. It is confirmed that the combination of artificial potential fields and MPC brings extra computational consumption, thereby resulting in the poorest real-time performance.

Table 1. Trajectory-tracking performance of different planning algorithms

Algorithms	Peak computation time (s)	Obstacle-state estimation convergence time (s)	Steady-state velocity estimation error (m/s)
STO-MPC	0.13	0.50	0.0015
GO-MPC	0.14	0.62	0.0021
APF-MPC	0.17	0.95	0.0034

In view of algorithm mechanisms and engineering applicability, STO-MPC is developed with a safety time-optimal objective. Solution complexity is reduced through the simplification of cost functions and constraint conditions, which renders it applicable to scenarios requiring rapid response. Global trajectory consistency is considered in the local optimization of GO-MPC. Despite a slight increase in computational burden, improved trajectory continuity and tracking precision are guaranteed. Although direct obstacle avoidance guidance is provided by APF-MPC via potential field principles, additional expenses caused by potential field calculation and nonlinear optimization restrict its popularization on low-power hardware platforms. Overall, STO-MPC exhibits the most prominent real-time capability and engineering adaptability among the three methods.

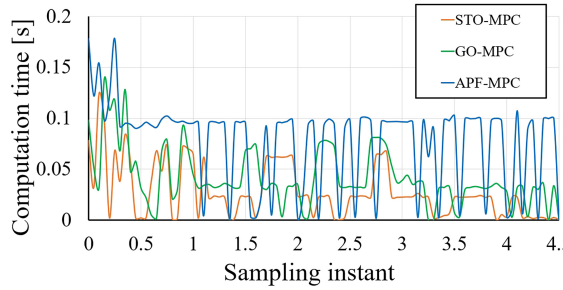


Fig. 9. Comparison of computation time for these three kinds of dynamic obstacle observers

The comparison of dynamic obstacle velocity estimation errors among the three algorithms is presented in Fig. 10, where evident performance differences can be observed. All three methods share an initial error of –0.02 m/s and achieve rapid convergence, while their convergence processes and steady-state fluctuation characteristics differ greatly. STO-MPC achieves the fastest convergence within approximately 0.5 s, with nearly zero steady-state error and negligible post-convergence fluctuations, thereby delivering superior estimation accuracy and stability. The convergence rate of GO-MPC is slightly lower than that of STO-MPC. Minor fluctuations occur after 0.5 s before gradual stabilization, and its steady-state error approaches zero. Although the overall performance is comparable, its dynamic response is relatively weaker. As for APF-MPC, the slowest convergence is obtained. Obvious periodic fluctuations arise from 0.5 s to 1 s,

indicating that extra disturbances are introduced by potential field calculation. Despite the final convergence of steady-state error, its dynamic stability is inferior to the other two algorithms.

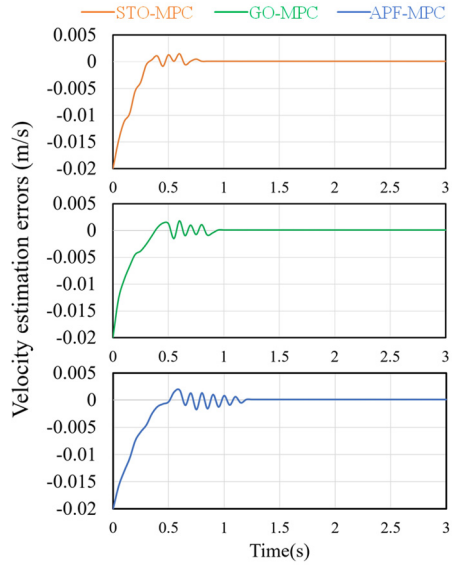


Fig. 10. Velocity estimation errors of the dynamic obstacle

From the perspective of algorithm mechanism, nonlinear disturbances during calculation are reduced by STO-MPC through the simplification of optimization objectives and constraints, leading to the fastest dynamic response and optimal steady-state performance in velocity estimation. Slight degradation in convergence speed is caused in GO-MPC, since extra constraints are adopted to maintain global trajectory consistency. Owing to the integration of the artificial potential field method, periodic interference is imposed on the velocity estimation of APF-MPC by nonlinear calculation and local optimum problems of potential fields, which induces obvious fluctuations during convergence. Although unbiased estimation can be realized ultimately, its dynamic performance is restricted. In summary, STO-MPC achieves the highest accuracy and stability in dynamic obstacle velocity estimation, followed by GO-MPC. Affected by the additional overhead of the integrated strategy, certain deficiencies in dynamic performance are exhibited by APF-MPC.

To quantitatively evaluate the trajectory tracking performance of the three algorithms, the root mean square error (RMSE), mean absolute error (MAE), and maximum absolute error (MaxAE) of the end-effector position and velocity estimation performance are calculated as shown in Table 2 and Table 3. As can be seen from Table 2, STO-MPC achieves the best trajectory tracking accuracy among the three algorithms. Its RMSE is 2.35 mm, which is 18.7 % lower than that of GO-MPC and 36.8 % lower than that of APF-MPC. The maximum tracking error of STO-MPC is also the smallest, indicating that it can maintain higher tracking accuracy even in the most challenging obstacle avoidance phase. This is mainly because the simplified optimization framework of STO-MPC reduces the computational delay, enabling more timely trajectory adjustment and thus improving tracking accuracy.

Table 2. Quantitative comparison of trajectory tracking performance

Type	RMSE (mm)	MAE (mm)	MaxAE (mm)
STO-MPC	2.35	1.87	5.62
GO-MPC	2.89	2.31	6.45
APF-MPC	3.72	2.98	8.13

ISSN PRINT 1392-8716, ISSN ONLINE 2538-8460

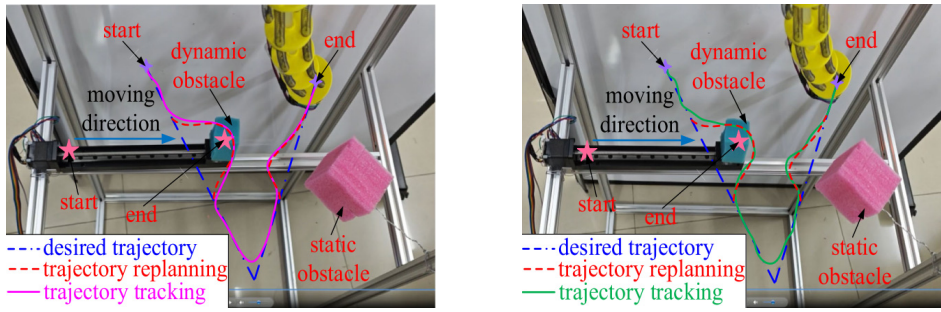
The quantitative results show that STO-MPC has the highest velocity estimation accuracy and the fastest convergence speed. Its RMSE is only 0.0032 m/s, and the estimation error converges to the steady-state value within 0.48 s. Compared with GO-MPC and APF-MPC, the convergence time is reduced by 22.6 % and 49.5 %, respectively, which verifies the superiority of STO-MPC in dynamic state estimation.

Table 3. Quantitative comparison of velocity estimation performance

Type	RMSE (m/s)	Convergence time (s)	Steady-state error (m/s)
STO-MPC	0.0032	0.48	0.0015
GO-MPC	0.0045	0.62	0.0021
APF-MPC	0.0068	0.95	0.0034

3.3. Comparative analysis of vibration suppression effects

For the research on trajectory tracking and dynamic obstacle avoidance of flexible robotic arms, V-shaped trajectories were selected for testing. A typical path containing uniform straight segments and sharp turns with high curvature is adopted to systematically verify the coupling performance of algorithms under the complete working conditions of dynamic obstacle approaching, collision avoidance steering and trajectory regression. Meanwhile, the robustness defects and vibration suppression capability of algorithms under multi-constraint conflicts and high-curvature motions can be effectively revealed. Compared with simple trajectories such as straight lines and circles, the V-shaped trajectory is highly consistent with the actual operation demands of feeding and obstacle avoidance in narrow industrial spaces. With moderate constraint intensity and outstanding performance differentiation, it can accurately distinguish comprehensive differences among various control algorithms in obstacle avoidance response, tracking accuracy and chattering suppression. Hence, an efficient and reliable test environment is provided for the comparative analysis of ADO-RITSMC, FNTSMC and other algorithms.



a) ADO-RITSMC b) FNTSMC

Fig. 11. Trajectory tracking results under different conditions.
Photo by the author in Qingdao on March 10, 2026

Trajectory tracking and dynamic obstacle avoidance results under diverse working conditions are illustrated in Fig. 11. Significantly superior performance in obstacle avoidance and trajectory tracking is demonstrated by ADO-RITSMC in comparison with FNTSMC. When confronting moving dynamic obstacles and fixed static obstacles, only smooth and slight local adjustments are implemented in the actual trajectory of ADO-RITSMC, which is highly fitted with reference and replanned paths. Precise safety avoidance is realized without unnecessary path deviation. By contrast, excessive obstacle avoidance behaviors are observed in FNTSMC, accompanied by larger trajectory deviation and tortuous returning paths, which reflects the conservatism defects of its response strategy. In terms of trajectory consistency and constraint adaptability, more prominent advantages are presented by ADO-RITSMC. The global tracking objective is steadily maintained throughout the movement, and a rapid and smooth return to the original path is

completed after obstacle avoidance. A stable safety distance from static obstacles is always guaranteed with smooth trajectory curvature and no oscillation. For FNTSMC, the global tracking target is lost during obstacle avoidance. Continuous deviations exist in the later-stage trajectory, and unstable sharp turns are generated near static obstacles, resulting in poorer comprehensive performance than ADO-RITSMC.

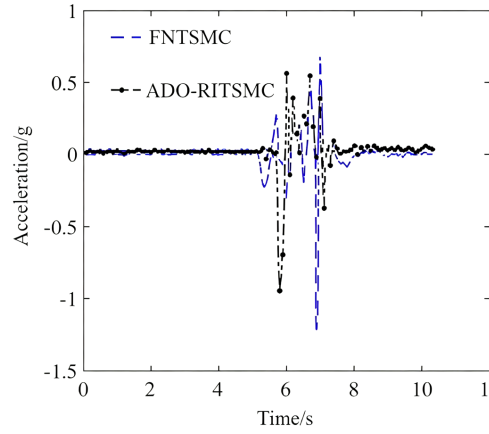


Fig. 12. Vibration acceleration test results under different conditions

The vibration suppression performances of the two control methods during trajectory tracking differ significantly, which can be directly verified through the vibration acceleration curves in Fig. 12. Vibration-suppression performance comparison is shown in Table 4. According to the experimental results, the peak vibration acceleration of FNTSMC reaches approximately –1.2 g, while that of ADO-RITSMC is only about –1.0 g, indicating a considerably larger vibration amplitude of the former. Moreover, the fluctuation duration near the peak is prolonged for FNTSMC, whereas the vibration of ADO-RITSMC decays more rapidly, which proves its superior capability in suppressing impact and chattering during the motion of flexible manipulators. Based on the dynamic model of the flexible manipulator, ADO is designed to achieve model-free real-time estimation of global disturbances through parameters such as observer gain matrices and adaptive gains. By designing a nonsingular integral terminal sliding mode surface, RITSMC is configured to achieve finite-time convergence of tracking errors within 0.1-0.5 s through parameters including terminal exponents, integral coefficients, and chattering suppression coefficients, while suppressing sliding mode chattering and elastic vibrations. Through their collaboration, the module is enabled to meet the core objectives of end-effector trajectory tracking accuracy.

Table 4. Vibration-suppression performance comparison

Control strategy	Peak vibration acceleration	Vibration amplitude reduction rate	Disturbance-suppression ratio
ADO-RITSMC	–1.0 g	16.7 %	> 90 %
FNTSMC	–1.2 g	–	Lower than 75 %

From the perspective of control principle, accurate estimation and compensation of internal and external disturbances are realized by ADO-RITSMC. Accordingly, the chattering phenomenon commonly existing in conventional sliding mode control is effectively weakened. Specifically, equivalent disturbances caused by dynamic obstacles, model uncertainties and external interferences are estimated and compensated in real time by ADO, which reduces the reliance of the controller on high-gain switching terms. Meanwhile, with the design of a non-singular terminal sliding mode surface, finite-time convergence is guaranteed by RITSMC,

and high-frequency switching of control inputs is reduced, thereby restraining the vibration induced by chattering at the source. In comparison, active disturbance compensation is not adopted in FNTSMC. Its switching gain must cover the full disturbance range, resulting in severe control chattering under dynamic working conditions such as obstacle avoidance. This is manifested as drastic fluctuations in vibration acceleration, which adversely affects the overall stability and trajectory tracking accuracy of the system.

4. Conclusions

1) The dynamic modeling and hierarchical control system of the flexible manipulator were completed. Through comparative experiments on three MPC trajectory planning algorithms, it was found that the minimum computational delay and the optimal dynamic response were achieved by STO-MPC with a simplified optimization framework. Outstanding performance in global trajectory consistency control was exhibited by GO-MPC, while poor real-time capability was presented by APF-MPC due to the nonlinear calculation limitation of potential fields. Effective obstacle avoidance in mixed obstacle environments was realized by all three algorithms, and STO-MPC was verified to possess the best comprehensive engineering adaptability.

2) According to the experimental results of obstacle velocity estimation, rapid convergence and negligible steady-state error were realized by STO-MPC, which was slightly affected by external computational disturbances. A slight attenuation of dynamic response was observed for GO-MPC. Periodic fluctuations were easily induced in APF-MPC by the coupling effect of potential fields, resulting in insufficient stability of dynamic state estimation. The critical effect of lightweight optimization design on improving the perception accuracy of dynamic environments was verified.

3) The results of high-curvature trajectory tests and vibration experiments confirmed that the elastic vibration of flexible links and control chattering were rapidly suppressed by the ADO-RITSMC strategy. Compared with the FNTSMC method, lower vibration peaks and shorter fluctuation durations were obtained. Smaller trajectory deviations and smoother path regression were guaranteed during obstacle avoidance. Adverse effects caused by parameter perturbations and sudden load variations were effectively overcome, and the dynamic control requirements of flexible manipulators with high precision and stability were fully satisfied.

4) Future work will focus on further improving the performance and applicability of the proposed control framework. Considering the coupling effects of multi-directional bending and torsional deformations of flexible manipulators, the extension of the STO-MPC and ADO-RITSMC framework to three-dimensional spatial trajectory tracking and obstacle avoidance tasks will be investigated. The integration of deep learning techniques with the proposed control strategy will be explored, such as using neural networks for online parameter optimization of the ADO and adaptive tuning of sliding mode gains, to further enhance the adaptability of the system to complex and unknown environments. Furthermore, dynamic simulations under various working conditions will be carried out to further verify the reliability of the proposed scheme.

Acknowledgements

The paper is supported by provincial scientific research projects (62874155).

Data availability

The datasets generated during and/or analyzed during the current study are available from the corresponding author on reasonable request.

Author contributions

Haiyan Sun: conceived and designed the research framework, constructed the dynamic model,

developed the STO-MPC trajectory replanning algorithm and ADO-RITSMC cooperative control strategy, and led the experimental design and data analysis, drafted and revised the manuscript. Yuanyuan Li: assisted in building the multi-sensor experimental platform, conducted comparative tests of O-shaped and V-shaped trajectories, collected and processed experimental data, participated in the optimization of control algorithms, and reviewed the manuscript.

Conflict of interest

The authors declare that they have no conflict of interest.

References

[1] X. Xia, Y. Sun, and J. Sun, "Dynamics and experiments of a tendon-actuated flexible robotic arm for capturing a floating target," *Defence Technology*, Vol. 47, pp. 216–241, Dec. 2024, https://doi.org/10.1016/j.dt.2024.12.013

[2] J. Liu, X. Li, M. Yin, L. Wei, and H. Wang, "Modeling and rotation control strategy for space planar flexible robotic arm based on fuzzy adjustment and disturbance observer," *Mathematics*, Vol. 12, No. 16, p. 2513, Aug. 2024, https://doi.org/10.3390/math12162513

[3] N. X. Chiem and P. X. Thuy, "A finite-time controller design based on Strick-feedback system for flexible joint manipulator," *International Journal of Control, Automation and Systems*, Vol. 23, No. 6, pp. 1829–1838, Jun. 2025, https://doi.org/10.1007/s12555-024-0939-4

[4] J. Kim, D. G. Nguyen, S. Park, M. Woo, D. Kim, and K. Han, "Data-driven vehicle torque vectoring control using streaming gaussian process MPC," *International Journal of Control, Automation and Systems*, Vol. 23, No. 12, pp. 3501–3512, Dec. 2025, https://doi.org/10.1007/s12555-025-0483-x

[5] S. Li, Q. Zhou, J. Jiang, X. Lu, and Z. Yu, "MPC-based motion control of AGV with improved A* and artificial potential field," *Proceedings of the Institution of Mechanical Engineers, Part D: Journal of Automobile Engineering*, Vol. 239, No. 4, pp. 1035–1044, Jul. 2024, https://doi.org/10.1177/09544070241264360

[6] N. Zhou, W. Deng, X. Yang, and J. Yao, "Continuous adaptive integral recursive terminal sliding mode control for DC motors," *International Journal of Control*, Vol. 96, No. 9, pp. 2190–2200, Sep. 2023, https://doi.org/10.1080/00207179.2022.2086928

[7] A. Alsaied, K. Li, J. Wang, and G. I. Y. Mustafa, "An optimal integral sliding mode control based time delay estimation for nonlinear lower limb exoskeleton robot," *Journal of Intelligent and Robotic Systems*, Vol. 112, No. 2, p. 34, Feb. 2026, https://doi.org/10.1007/s10846-026-02366-0

[8] A. L. Silva and D. A. Santos, "Fast nonsingular terminal sliding mode flight control for multirotor aerial vehicles," *IEEE Transactions on Aerospace and Electronic Systems*, Vol. 56, No. 6, pp. 4288–4299, Apr. 2020, https://doi.org/10.1109/taes.2020.2988836

[9] R. Sengalani and S. Rasool Mohideen, "Vibration control using a modern control system for hybrid composite flexible robot manipulator arm," *Journal of Automation, Mobile Robotics and Intelligent Systems*, Vol. 16, No. 2, pp. 36–45, Jun. 2023, https://doi.org/10.14313/jamris/2-2022/14

[10] M. Efafi, S. A. A. Hosseini, and H. Tourajizadeh, "Robust control and vibration reduction of a 3D nonlinear flexible robotic arm," *Iranian Journal of Science and Technology, Transactions of Mechanical Engineering*, Vol. 46, No. 4, pp. 1157–1173, Jan. 2022, https://doi.org/10.1007/s40997-021-00484-8

[11] F. A. Raheem, A. F. Hasan, E. H. Flaieh, and A. J. Humaidi, "A nonlinear disturbance observer-based super-twisting sliding mode controller for a knee-assisted exoskeleton robot," *Automation*, Vol. 7, No. 1, p. 23, Jan. 2026, https://doi.org/10.3390/automation7010023

[12] A. H. Hameed, S. A. Al-Samarraie, and A. J. Humaidi, "Active unmatched disturbance rejection quasi-sliding observer for electronic throttle valve system based on backstepping control," *Journal of Engines*, Vol. 18, No. 2, pp. 195–211, Apr. 2025, https://doi.org/10.4271/03-18-02-0011

[13] A. H. Hameed, S. A. Al-Samarraie, and A. J. Humaidi, "Backstepping-based nonlinear disturbance observer for speed control of DC motor," in *AIP Conference Proceedings*, Vol. 3232, p. 030007, Oct. 2024, https://doi.org/10.1063/5.0236229

[14] C. Pany and G. Li, "Editorial: application of periodic structure theory with finite element approach," *Frontiers in Mechanical Engineering*, Vol. 9, No. 9, p. 1192657, Apr. 2023, https://doi.org/10.3389/fmech.2023.1192657

[15] C. Pany, "Determination of bounding frequencies of cylindrical shells using a periodic structure wave approach with Rayleigh-Ritz method," *Journal of Engineering Sciences*, Vol. 30, No. 5, pp. 679–685, May 2024, https://doi.org/10.5505/pajes.2023.93765

[16] M. Alshihabi, M. Ozkahraman, and M. Y. Kayacan, "Enhancing the reliability of a robotic arm through lightweighting and vibration control with modal analysis and topology optimization," *Mechanics Based Design of Structures and Machines*, Vol. 53, No. 3, pp. 1950–1974, Mar. 2025, https://doi.org/10.1080/15397734.2024.2400207

[17] P. Sarkhel, N. Banerjee, and N. B. Hui, "Fuzzy logic-based tuning of PID controller to control flexible manipulators," *SN Applied Sciences*, Vol. 2, No. 6, pp. 367–377, May 2020, https://doi.org/10.1007/s42452-020-2877-y

[18] X. Yang, S. S. Ge, and W. He, "Dynamic modelling and adaptive robust tracking control of a space robot with two-link flexible manipulators under unknown disturbances," *International Journal of Control*, Vol. 91, No. 4, pp. 969–988, Apr. 2018, https://doi.org/10.1080/00207179.2017.1300837

[19] J. Yang, W.-H. Chen, and S. Li, "Non-linear disturbance observer-based robust control for systems with mismatched disturbances/uncertainties," *IET Control Theory and Applications*, Vol. 5, No. 18, pp. 2053–2062, Dec. 2011, https://doi.org/10.1049/iet-cta.2010.0616

[20] H. Zhang, D. Zhu, C. Liu, and Z. Hu, "Tracking fault-tolerant control based on model predictive control for human occupied vehicle in three-dimensional underwater workspace," *Ocean Engineering*, Vol. 249, p. 110845, Mar. 2022, https://doi.org/10.1016/j.oceaneng.2022.110845

[21] V. M. Hernández-Guzmán and J. Orrante-Sakanassi, "Global PID control of robot manipulators equipped with PMSMs," *Asian Journal of Control*, Vol. 20, No. 1, pp. 236–249, Jun. 2017, https://doi.org/10.1002/asjc.1532

[22] J. Zhang, X. Dai, Q. Huang, and Q. Wu, "AILC for rigid-flexible coupled manipulator system in three-dimensional space with time-varying disturbances and input constraints," *Actuators*, Vol. 11, No. 9, p. 268, Sep. 2022, https://doi.org/10.3390/act11090268

[23] M. H. Korayem, H. Esfandiar, and R. Dargahi, "Determining load carrying capacity of a manipulator by game theory: closed-loop nonzero-sum differential game approach," *Journal of Mechanical Science and Technology*, Vol. 30, No. 11, pp. 5197–5205, Nov. 2016, https://doi.org/10.1007/s12206-016-1037-1



Haiyan Sun is an Associate Professor in Qingdao Huanghai University. She received her graduate degree from Shandong University of Science and Technology, Shandong, 2013, China. Her current research interests include computer science and simulation, mechanical engineering, etc.



Yuanyuan Li is An Associate Professor in Qingdao Huanghai University. She received her graduate degree from Shandong University of Science and Technology, Shandong, 2012, China. Her current research interests include mechanical engineering, etc.